PERGAMON

International Journal of Solids and Structures 40 (2003) 2017–2035

INTERNATIONAL JOURNAL OF SOLIDS and STRUCTURES

www.elsevier.com/locate/ijsolstr

Three-dimensional stress analyses in composite laminates with an elastically pinned hole

B. Yang [a], E. Pan [a], F.G. Yuan [b,*]

[a] *Structures Technology, Inc., 543 Keisler Dr., Suite 204, Cary, NC 27511, USA*

[b] *Department of Mechanical and Aerospace Engineering, North Carolina State University, Raleigh, NC 27695, USA*

Received 26 December 2001; received in revised form 23 September 2002

Abstract

We present a three-dimensional (3-D) stress analysis for composite laminates with an elastically pinned circular hole. The effects of friction, bearing force and bypass loading on the stress redistribution are studied in detail. The numerical approach is based on a multilayer boundary element method (MLBEM), a non-traditional BEM particularly designed for anisotropic composite laminates, coupled with the traditional BEM for the pin filling the hole. The unique characteristic of the MLBEM is that the fundamental solution employs Green's functions that satisfy the interfacial continuity conditions and top- and bottom-surface traction-free and symmetry conditions. This fundamental solution allows us to design a BE scheme without involving discretization on the interfaces and surfaces unless the laminates are imposed by different boundary conditions. Consequently, in this case of pinned joint, only the hole surface among the composite boundary and interfaces needs to be discretized. A Coulomb-type friction law is used to simulate the frictional contact interaction between the composite and pin. To solve the frictional contact problem, an iterative scheme of successive over-relaxation has been proposed where the contact location and frictional contact condition are determined at the same time in the iteration solution. By applying the MLBEM, stress analyses are performed for a laminate plate with the stacking sequence $(0/\mp 45/\overline{90})_s$. The issues of engineering interests, such as the loading-sequence and cycling dependencies of stress state due to the presence of friction, are addressed. The solutions, shown by complicated contact maps and stress states around the hole, suggested that a 3-D approach to pinned composite joints is necessary for the interpretation of the underlying physics.

Keywords: Three-dimensional stress analysis; Composite laminates; Bolted joint; Bearing and bypass loading; Frictional contact; Boundary element method

1. Introduction

Owing to their unique light weight/high strength feature, composite laminates have been extensively used in various engineering structures, in particular, in aircraft and space structures. The structural composites

* Corresponding author. Tel.: +1-919-515-5947; fax: +1-919-515-5934.
E-mail address: yuan@eos.ncsu.edu (F.G. Yuan).

0020-7683/02/$ - see front matter © 2002 Published by Elsevier Science Ltd.
doi:10.1016/S0020-7683(02)00523-1

are commonly jointed by fastening, bonding, or a combination of these two for transferring load from one component to the other. Each joint method has its own advantages and deficiencies (Lubin, 1982; Schwartz, 1984).

It is well known that stress concentrations near the fastener holes could initiate delamination or other types of damage modes, which could then lead to final failure (Persson et al., 1998). Apart from the experimental approach (e.g., Daniel et al., 1974), various analytical methods have been proposed to examine the stress field around an open hole, such as the boundary layer method (Tang, 1977, 1979), the linear laminate finite element method (FEM) (Waszczak and Cruse, 1971; Soni, 1981), the three-dimensional (3-D) discrete layer FEM (Rybicki and Hopper, 1973; Rybicki and Schmuesser, 1976; Nishioka and Atluri, 1982; Raju and Crews, 1982), and the spline variational method (Iarve, 1996). More recently, an efficient and accurate *non-traditional* multilayer boundary element method (MLBEM) has been proposed by the authors for the stress analysis around an open hole in composite laminates (Pan et al., 2001).

The mechanical behavior of a composite laminate structure with filled mechanical fastener is more complicated than that in the open hole case. While a comprehensive review was given by Camanho and Matthews (1997), an experimental program was conducted by Ireman et al. (2000) in order to measure and characterize the development of damage in the vicinity of fastener holes in graphite/epoxy composite laminates. Also, several simplified models were proposed to numerically study the stress field and failure processes in mechanically fastened joints in composite laminates. For example, Dano et al. (2000) proposed a two-dimensional (2-D) FEM model to predict the response of fastener-loaded composite plate, where the fastener is assumed to be rigid. The traditional 2-D BEM has also been proposed recently to analyze similar problems by Lie et al. (2000) and Lin et al. (2000), with the fastener treated as a one-dimensional spring in the former and as a rigid medium in the latter. The 3-D FEM analyses were carried out by Chen et al. (1995), Ireman (1998), and Persson et al. (1998). In these studies, the fastener was assumed to be elastic and no friction was allowed along the interface between the fastener and composite except the study by Ireman (1998). In a similar study, Iarve (1997) proposed a B-spline approximation approach with no-friction assumption. On the other hand, Marshall et al. (1989) using the FEM concluded that the pin-hole contact friction is as equally important as the laminate stiffness to the stress and failure behavior of composite laminates.

In this article, we propose an efficient and accurate numerical method for the analysis of the mechanical behavior of a composite laminate plate with an elastic fastener in a circular hole under a bearing force on the fastener and/or a bypass loading in the composite. Each ply of the composite laminates is assumed to be generally anisotropic. The fastener is considered as isotropic. The interfaces between the lamina plies are assumed to be perfectly bonded. The interaction between the composite and fastener is followed by a Coulomb-type friction law. The problem is solved by using a novel 3-D boundary element formulation, in which the fundamental solution satisfies the interfacial continuity conditions and the traction-free and symmetry conditions on the top and bottom surfaces (Yuan et al., in press; Pan et al., 2001; Yang and Pan, 2002). Consequently, only the hole surface of the composite plate needs to be discretized. This leads to a substantial reduction of the numerical approximations and the resulting system of discretized equations is much smaller compared to that in the FEM and the conventional BEM. To simulate the nonlinear interaction and predict the unknown frictional contact zone between the composite and the pin, an efficient iterative scheme of successive over-relaxation is proposed. Numerical examples are then carried out for a laminate plate with the stacking sequence $(0/\mp 45/\overline{90})_s$. It is shown that a finite friction coefficient along the hole has substantial effects on the stress redistribution. It is further shown that the contact stress state in different plies can be very different due to the stiffness difference in the plies. This suggested that a 3-D approach of the laminate pinned joint is necessary. Finally, we observed that the loading sequence (first bearing force and then bypass loading, and vice versa) and cycling has only a slight influence on the final stress distribution in the case of perfect fitting between the hole and pin.

2. Problem formulation

2.1. Problem

We consider a composite laminate plate with a circular hole, as shown in Fig. 1a. The plate thickness is denoted by H, and the length and width by L and W respectively. The left lateral surface of the plate is fixed. The right lateral surface is attached to a rigid block, which can move without rotation uniaxially. The hole of radius R is filled with a cylindrical pin without clearance. The other parts of the plate surface are free of traction. The pin, which symmetrically stick out of the plate surfaces, are fixed at the ends. The lateral surface is initially free of traction and may partially turn in contact with the hole surface upon loading.

Initially, the plate and pin are in the stress-free state. Upon a uniaxial force T applied to the rigid block, the plate is loaded, and consequently the hole surface is displaced and partially turns in contact with pin surface. The resulting displacement at the right lateral surface of the plate is denoted by U. The resulting force between the plate and pin is denoted by $2F$, and called a bearing force. A bypass straining on the system is defined as U/L. An equivalent bypass loading is defined as $(T-F)/W$. If $W \gg R$, the magnitude of F should become trivial relative to that of T. Also, if $L \gg R$, the force T should be distributed uniformly in the horizontal direction on the right lateral surface of the plate. When all these conditions hold and our interest focuses on the local stress field around the hole, the above configuration, often found in laboratory tests, may be simulated by an infinite laminate plate problem, as described next.

Consider an infinite laminate plate with a pinned circular hole, as shown in Fig. 1b. A Cartesian coordinate system, (x_1, x_2, x_3), and a cylindrical coordinate system, (r, θ, x_3), with $r = (x_1^2 + x_2^2)^{1/2}$ and $\theta = \tan^{-1}(x_2/x_1)$, are established. The origin is located at the hole center on the plate bottom surface. The pin is assumed to be isotropic and linearly elastic. The laminates are assumed to be anisotropic and linearly elastic and are generally dissimilar from one another. The interfaces between the laminae are perfectly bonded. This system is initially in the stress-free state. The laminate plate is then subjected to a remote uniform straining, $\varepsilon_{11}^{\infty}$, together with zero stress components σ_{3i}^{∞} $(i = 1, 2, 3)$ and zero average stress components σ_{12}^{∞} and σ_{22}^{∞} over the laminae. By applying the classical laminate theory, where the condition of uniform fields in each lamina and condition of continuous in-plane strain components across an interface are imposed, these remote fields, $\boldsymbol{\sigma}^{\infty}$ and $\boldsymbol{\epsilon}^{\infty}$, which are assumed to be unaffected by the hole deformation, can be determined for every lamina completely. Corresponding to the previous configuration, $\varepsilon_{11}^{\infty} = U/L$. In addition, the pin is pushed against the hole surface by a symmetric load of $2F$, F on each end. Friction between the hole and pin surfaces is considered and the interaction is followed by a Coulomb-type friction law. When the friction is present, the loading sequence of applying $\varepsilon_{11}^{\infty}$ and F may affect the stress state in the laminates. In the case, cycling of the loads may also play a role in redistributing the stress field, exhibiting a loading-history effect.

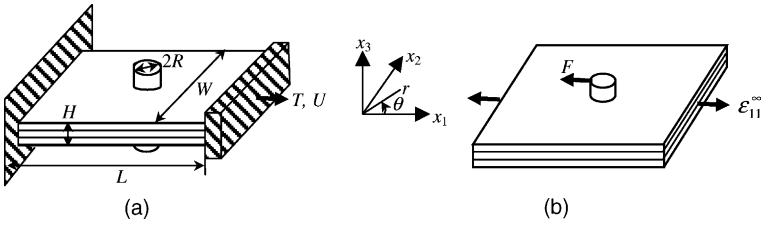

Fig. 1. Composite laminates with an elastically pinned circular hole: (a) a finite geometry; (b) an infinite plate approaching (a). A Cartesian coordinate system, (x_1, x_2, x_3), and a cylindrical coordinate system, (r, θ, x_3), are established for the plate and pin system.

2.2. Boundary integral-equation formulation

A boundary integral-equation (BIE) formulation is used to describe the mechanical behavior of the composite system coupled with an elastic pin through frictional contact. The displacement $u_i^{(c)}$ at a point $\mathbf{X}$ in the laminate plate can be expressed by an integral of weighted displacement $u_j^{(c)}$ and traction $p_j^{(c)}$ along the plate boundary $S^{(c)}$, as

$$c(\mathbf{X})[u_i^{(c)}(X) - u_i^{\infty}(X)] = \int_{S^{(c)}} \{u_{ij}^{*(c)}(X,\mathbf{x})[p_j^{(c)}(\mathbf{x}) - p_j^{\infty}(\mathbf{x})] - p_{ij}^{*(c)}(X,\mathbf{x})[u_j^{(c)}(\mathbf{x}) - u_j^{\infty}(\mathbf{x})]\}\,\mathrm{d}S(\mathbf{x}), \tag{1}$$

where $c(\mathbf{X}) = 1$ if $\mathbf{X}$ is interior, and 0.5 if $\mathbf{X}$ on the boundary (except at the corners), u_j^{∞} and p_j^{∞} are the homogeneous solutions in the plate (if without the hole) under the far-field straining, and the repeated subscript index implies the conventional summation over its range unless suspended explicitly. In addition, $u_{ij}^{*(c)}$ and $p_{ij}^{*(c)}$ are the fundamental solutions of displacement and traction specially designed for anisotropic composite laminates, as summarized in Appendix A (Yuan et al., in press; Pan et al., 2001; Yang and Pan, 2002).

It should be remarked that the above fundamental solutions (i.e., Green's functions), derived within the framework of extended Stroh formalism and Fourier transforms, can be designed to specifically satisfy the traction-free (and/or symmetry) conditions on the plate surfaces as well as the continuity conditions of displacement and traction across the interfaces. Because the surfaces where the boundary conditions are satisfied in the fundamental solutions do not need discretization in the BIE formulation using these solutions as integral kernels, the effective boundary, $S^{(c)}$, can then be reduced to the hole surface in the present problem of pinned joint. Consequently, the numerical approximations in the BEM to solve the laminate plate problem are reduced significantly in comparison to the conventional BEM and other domain-based FEM (Pan et al., 2001).

Similarly, the displacement $u_i^{(p)}$ at an arbitrary point in the pin can be expressed by an integral of weighted displacement $u_j^{(p)}$ and traction $p_j^{(p)}$ along the pin boundary $S^{(p)}$, as

$$c(\mathbf{X})u_i^{(p)}(X) = \int_{S^{(p)}} \{u_{ij}^{*(p)}(X,\mathbf{x})p_j^{(p)}(\mathbf{x}) - p_{ij}^{*(p)}(X,\mathbf{x})u_j^{(p)}(\mathbf{x})\}\,\mathrm{d}S(\mathbf{x}), \tag{2}$$

where $c(\mathbf{X})$ means in the same way as above for the laminate plate, and $u_{ij}^{*(p)}$ and $p_{ij}^{*(p)}$ are the Kelvin's fundamental solutions of displacement and traction respectively for linear isotropic elastic solids in full space (Love, 1944; Brebbia et al., 1984).

The fields $(\mathbf{u}^{(c)}, \mathbf{p}^{(c)})$ in the composite and $(\mathbf{u}^{(p)}, \mathbf{p}^{(p)})$ in the pin are separated unless the hole and pin surfaces turn in contact. When it prevails, these fields, and thus Eqs. (1) and (2), are coupled through a law that describes the contact interaction. In this work, a Coulomb-type friction law is considered, as described next. The coupling of Eqs. (1) and (2) by the friction law, and its numerical implementation, will be described in a later section.

2.3. Frictional contact

The frictional contact between the hole and pin surfaces is modeled by a local Coulomb-type friction law. Suppose that two smooth surfaces are in conformal contact at a reference point $\mathbf{x}$, as shown in Fig. 2. The two opposite physical points that are in contact at $\mathbf{x}$ are distinguished by designating respectively as the master and slave points, $\mathbf{x}^+$ and $\mathbf{x}^-$. The corresponding surfaces are called the master and slave surfaces, respectively. The local Cartesian coordinate system, (n, t_1, t_2), is established with the origin located at $\mathbf{x}$. The normal axis, n, coincides with the outward normal of the master surface at $\mathbf{x}^+$.

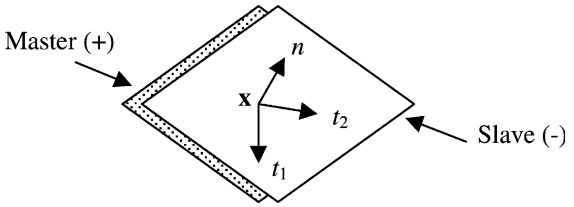

Fig. 2. Two smooth surfaces in conformal frictional contact at point **x**, as designated as the master (+) and slave (−) surfaces respectively. A local Cartesian coordinate system, (n, t_1, t_2) is established, with n being the outward normal of the master surface at **x**.

The non-penetration condition of the master and slave surfaces requires

$$w_n(\mathbf{x}) \geqslant 0, \tag{3}$$

where w_n is the normal component of displacement difference across the surfaces, $\mathbf{w}(\mathbf{x}) \equiv \mathbf{u}(\mathbf{x}^-) - \mathbf{u}(\mathbf{x}^+)$. If the surfaces are in contact, $w_n = 0$. If they are separated, $w_n > 0$. When the separation occurs, the surfaces are assumed to be in traction-free condition.

When the surfaces are in contact, i.e., $w_n = 0$, a Coulomb-type friction law is assumed to describe the frictional interaction between them, written by

$$p_\alpha = -f p_n \frac{\mathrm{d}w_\alpha}{\mathrm{d}s}, \tag{4}$$

where the Greek subscript α takes value from 1 to 2, corresponding to the local tangential coordinates t_1 and t_2 respectively, f is the static friction coefficient, and $s \equiv |\mathbf{w}|$. The law states that the frictional shear traction is proportional to the pressure $(-p_n)$ in magnitude, and opposite to the tangent of relative sliding displacement trajectory. Due to the dependence of the frictional force on trajectory tangent of relative displacement, a loading-history effect is inherent in the present formulation of the pinned composite joint.

3. Iterative boundary element method of successive over-relaxation

3.1. Mesh and discrete boundary element equations

The fundamental solution for laminate plate containing dissimilar plies, used in the present BIE formulation, satisfies the continuity conditions of displacement and traction across the interfaces and the traction-free and/or symmetry conditions on the top and bottom surfaces (Yuan et al., in press; Pan et al., 2001; Yang and Pan, 2002). The partial satisfaction of interfacial and boundary conditions in the fundamental solution allows us to design a BE scheme without involving discretization on those interfaces and surfaces unless the laminates are imposed by a different boundary condition. Thus, in the present case of pinned joint, only the hole surface among the plate surfaces needs to be discretized. Meanwhile, because the Kelvin's fundamental solution used in the BIE formulation of the pin refers to the full space, the entire boundary of the pin needs to be discretized. All of the elements are of the constant type, assuming uniform fields within each element and a single node located at the center. Note that the elements and nodes on the hole surface match with those on the vertical surface of the pin. The nodes on the hole surface and those on the pin surface are numbered separately.

A field quantity, $\mathbf{q}(\mathbf{x})$, in each of the constant elements may be approximated by the nodal value, $\mathbf{q}^n$, at the element center, written as

$$\mathbf{q}(\mathbf{x}) = \mathbf{q}^n, \quad \text{as } \mathbf{x} \in \text{the } n\text{th element.} \tag{5}$$

By substituting the approximations for displacement and traction into Eqs. (1) and (2), a discrete version of these BIEs are obtained, namely, the discrete BE equations, as

$$c(\mathbf{X}^m)[u_i^{(\mathrm{c})m} - u_i^{\infty m}] = \sum_{n=1}^{N^{(\mathrm{c})}} [g_{ij}^{(\mathrm{c})mn}(p_j^{(\mathrm{c})n} - p_j^{\infty n}) - h_{ij}^{(\mathrm{c})mn}(u_j^{(\mathrm{c})n} - u_j^{\infty n})], \tag{6}$$

$$c(\mathbf{X}^m)u_i^{(\mathrm{p})m} = \sum_{n=1}^{N^{(\mathrm{p})}} [g_{ij}^{(\mathrm{p})mn} p_j^{(\mathrm{p})n} - h_{ij}^{(\mathrm{p})mn} u_j^{(\mathrm{p})n}], \tag{7}$$

where $N^{(\mathrm{c})}$ and $N^{(\mathrm{p})}$ are the total numbers of nodes for the composite plate and the pin respectively, and the conventional summation over repeated index does not apply to the superscript indices. The influence coefficients, g_{ij}^{mn} and h_{ij}^{mn}, are given by

$$g_{ij}^{mn} = \int_{S^n} u_{ij}^*(\mathbf{X}^m, \mathbf{x})\, \mathrm{d}S(\mathbf{x}), \tag{8}$$

$$h_{ij}^{mn} = \int_{S^n} p_{ij}^*(\mathbf{X}^m, \mathbf{x})\, \mathrm{d}S(\mathbf{x}), \tag{9}$$

valid for both of the composite plate and pin, where S^n is the element where the nth node is located. The above equations can be evaluated analytically for a constant element for the isotropic elastic pin (Kuriyama et al., 1995). However, their evaluation for the anisotropic laminate plate has to be carried out numerically and this is complicated by involving multidimensional integrals and various singularities (Pan et al., 2001; Yang and Pan, 2002).

If the source point, $\mathbf{X}^m$ is located on the boundary, Eqs. (6) and (7) then involve boundary quantities only and can be used to formulate a numerical scheme to solve the problem given appropriate boundary and initial conditions. The initial condition is needed due to the involvement of virtual time derivative (i.e., tangent derivative of a particle trajectory) in the description of the frictional contact (Eq. (4)). In the present work, an iterative scheme of successive over-relaxation is developed to solve the complicated problem of 3-D frictional contact between different bodies, based on the previous work by Yang and Ravi-Chandar (1998), as described next.

3.2. Iterative scheme of successive over-relaxation

Without knowing the contact zone a priori, the present problem of coupled laminate plate and pin generally requires an iterative procedure to determine the contact zone under the non-penetration condition (Eq. (3)), not to mention the coupling of tangential traction components to normal traction component under the Coulomb-type friction law (Eq. (4)). In the literature, to the best knowledge of the authors, the fast iterative methods developed for medium- and large-scale BE computations (e.g., Merkel et al., 1998) are all for systems without altering the stiffness matrix during the solution process, and hence inapplicable to the present problem involving the Coulomb-type frictional contact between different bodies. Yang and Ravi-Chandar (1998) have presented an iterative BE scheme of successive over-relaxation for 2-D single-body elastostatic problems with similar frictional contact between crack surfaces. Applying the scheme, Yang et al. (2001) have simulated the fatigue crack growth in a 2-D specimen subjected to thousands of cycles of fatigue loading at a tolerable cost of CPU time on the moderate-power Personal Computer. However, the examples they have solved are in a relatively small size of about 200 nodes. In the following, this method is modified to handle the more complicated 3-D problem in a much larger computational size by one order.

Let $(\mathbf{u}^{(c)}, \mathbf{p}^{(c)})$ and $(\mathbf{u}^{(p)}, \mathbf{p}^{(p)})$ be the trial sets of displacement and traction on the boundaries of the plate and pin, respectively. Substituting them into Eqs. (6) and (7) (now, with $\mathbf{X}^m$ located at one of the nodes, and hence $c = 0.5$), these equations would not be satisfied in general; instead, one obtains the following residuals:

$$r_i^{(c)m} = \sum_{n=1}^{N^{(c)}} [g_{ij}^{(c)mn}(p_j^{(c)n} - p_j^{\infty n}) - h_{ij}^{(c)mn}(u_j^{(c)n} - u_j^{\infty n})] - 0.5(u_i^{(c)m} - u_i^{\infty m}), \quad m = 1, 2, \ldots, N^{(c)}, \tag{10}$$

$$r_i^{(p)m} = \sum_{n=1}^{N^{(p)}} [g_{ij}^{(p)mn} p_j^{(p)n} - h_{ij}^{(p)mn} u_j^{(p)n}] - 0.5 u_i^{(p)m}, \quad m = 1, 2, \ldots, N^{(p)}. \tag{11}$$

If the residuals all are sufficiently close to zero, the trial sets of $(\mathbf{u}^{(c)}, \mathbf{p}^{(c)})$ and $(\mathbf{u}^{(p)}, \mathbf{p}^{(p)})$ represent an approximate solution to the problem of the coupled laminate plate and pin. Depending on the boundary conditions to be prescribed, the following scheme is developed to determine the unknown displacement and traction components iteratively.

Two types of boundary conditions are encountered in the present problem. One is the regular boundary condition of displacement, traction, or mixed displacement and traction components. The other is the contact and separation condition, described by Eqs. (3) and (4), as well as the traction-free condition associated with the separation mode. This second condition is needed at the matching nodes between the hole and pin surfaces. For the nodes under the regular boundary condition, the displacement component, $u_i^{m,l+1}$, if not prescribed as a boundary condition, is calculated by using the results of the lth iteration step by

$$u_i^{m,l+1} = u_i^{m,l} + \omega r_i^m(\mathbf{u}, \mathbf{p})/(0.5 + h_{ii}^{mm}) \quad \text{(no sum on } i\text{)}, \tag{12}$$

where ω is an adjustable factor of relaxation. Similarly, the traction component, $p_i^{m,l+1}$, if not prescribed as a boundary condition, is calculated by

$$p_i^{m,l+1} = p_i^{m,l} - \omega r_i^m(\mathbf{u}, \mathbf{p})/g_{ii}^{mm} \quad \text{(no sum on } i\text{)}. \tag{13}$$

The residual, $r_i^m(\mathbf{u}, \mathbf{p})$, is computed by using the nodal values at the $(l+1)$th iteration step if available, or at the lth iteration step. Note that the above expressions (Eqs. (12) and (13)) are valid for nodes on both of the composite plate and the pin.

For the matching nodes between the hole and pin surfaces, either the contact or the separation mode may be activated. If the contact mode prevails, the equality in Eqs. (3), and (4), are invoked as the boundary condition at the pair of matching nodes. Otherwise, in the separation mode the traction-free condition is imposed. For convenience, the local coordinate system, with the normal direction coincident with the outward normal of the master surface (Fig. 2), is used in the contact case. Furthermore, the master node is always taken to be on the hole surface, while the slave node to be on the pin surface. In practice, whether the contact at a pair of matching nodes occurs is determined by the sign of the master-nodal normal traction component $p_n^{(mas)}$ $(= -p_n^{(sla)})$ at the lth iterative step: If $p_n^{(mas),l} < 0$, pressure is present and thus the contact is assumed to occur between the pair of matching nodes. In this case, the normal traction $p_n^{(mas)}$ at the $(l+1)$th iteration step is computed by

$$p_n^{(mas),l+1} = p_n^{(mas),l} - \omega[r_n^{(c)mm}(\mathbf{u}^{(c)}, \mathbf{p}^{(c)}) - r_n^{(p)ss}(\mathbf{u}^{(p)}, \mathbf{p}^{(p)})]/(g_{nn}^{(c)mm} + g_{nn}^{(p)ss}), \tag{14}$$

where the superscript m refers to the master-node number, and the superscript s to the slave-node number. Also, the master-nodal normal displacement component, $u_n^{(mas)}$ $(= u_n^{(sla)}$, due to Eq. (3)) at the $(l+1)$th iteration step is computed by

$$u_n^{(mas),l+1} = u_n^{(mas),l} + \omega[r_n^{(c)mm}(\mathbf{u}^{(c)}, \mathbf{p}^{(c)}) + r_n^{(p)ss}(\mathbf{u}^{(p)}, \mathbf{p}^{(p)})]/(1 + h_{nn}^{(c)mm} + h_{nn}^{(p)ss}). \tag{15}$$

Furthermore, in the tangential directions, the sum of the master-nodal and slave-nodal displacement components at the $(l+1)$th iteration step is computed by

$$u_\alpha^{(\mathrm{mas}),l+1}+u_\alpha^{(\mathrm{sla}),l+1}=u_\alpha^{(\mathrm{mas}),l}+u_\alpha^{(\mathrm{sla}),l}+2\omega[r_\alpha^{(\mathrm{c})mm}(\mathbf{u}^{(\mathrm{c})},\mathbf{p}^{(\mathrm{c})})+r_\alpha^{(\mathrm{p})ss}(\mathbf{u}^{(\mathrm{p})},\mathbf{p}^{(\mathrm{p})})]/(1+h_{\alpha\alpha}^{(\mathrm{c})mm}+h_{\alpha\alpha}^{(\mathrm{p})ss}) \quad (\text{no sum on } \alpha). \tag{16}$$

Meanwhile, the difference of the displacement components at the $(l+1)$th iteration step is computed by

$$-u_\alpha^{(\mathrm{mas}),l+1}+u_\alpha^{(\mathrm{sla}),l+1}=-u_\alpha^{(\mathrm{mas}),l}+u_\alpha^{(\mathrm{sla}),l}+2\omega[-r_\alpha^{(\mathrm{c})mm}(\mathbf{u}^{(\mathrm{c})},\mathbf{p}^{(\mathrm{c})})+r_\alpha^{(\mathrm{p})ss}(\mathbf{u}^{(\mathrm{p})},\mathbf{p}^{(\mathrm{p})})]/[1+h_{\alpha\alpha}^{(\mathrm{c})mm}+h_{\alpha\alpha}^{(\mathrm{p})ss}-(g_{\alpha\alpha}^{(\mathrm{c})mm}+g_{\alpha\alpha}^{(\mathrm{p})ss})fp_n^{(\mathrm{mas}),l+1}/s_f^l] \quad (\text{no sum on } \alpha), \tag{17}$$

with

$$s_f^l=\begin{cases} s_{fc} & \text{if } \Delta s<s_{fc},\\ \Delta s & \text{otherwise,}\end{cases} \tag{18}$$

where $\Delta s=s^l-s^{(0)}$, in which $s^{(0)}$ is at a previous (reference) "time" step, and s_{fc} is a numerical parameter, for instance, taken to be around one ten-thousandth of the average magnitude of Δs. From the computed sum and difference, the tangential displacement components at the master and slave nodes can be obtained. Furthermore, the master-nodal tangential traction component $p_\alpha^{(\mathrm{mas})}$ $(=-p_\alpha^{(\mathrm{sla})})$ at the $(l+1)$th iteration step is computed, in the discrete form of Eq. (4), by

$$p_\alpha^{(\mathrm{mas}),l+1}=-fp_n^{(\mathrm{mas}),l+1}(w_\alpha^{l+1}-w_\alpha^{(0)})/s_f^l. \tag{19}$$

If the previously computed $p_n^{(\mathrm{mas}),l}\geqslant 0$ or updated $p_n^{(\mathrm{mas}),l+1}\geqslant 0$, the separation mode between the pair of matching nodes is activated. In this case, the sum of master-nodal and slave-nodal displacement components at the $(l+1)$th iteration step is computed by

$$u_i^{(\mathrm{mas}),l+1}+u_i^{(\mathrm{sla}),l+1}=u_i^{(\mathrm{mas}),l}+u_i^{(\mathrm{sla}),l}+2\omega[r_i^{(\mathrm{c})mm}(\mathbf{u}^{(\mathrm{c})},\mathbf{p}^{(\mathrm{c})})+r_i^{(\mathrm{p})ss}(\mathbf{u}^{(\mathrm{p})},\mathbf{p}^{(\mathrm{p})})]/(1+h_{ii}^{(\mathrm{c})mm}+h_{ii}^{(\mathrm{p})ss}). \tag{20}$$

Meanwhile, the difference of master- and slave-nodal displacement components at the $(l+1)$th iteration step is computed by

$$-u_i^{(\mathrm{mas}),l+1}+u_i^{(\mathrm{sla}),l+1}=-u_i^{(\mathrm{mas}),l}+u_i^{(\mathrm{sla}),l}+2\omega[-r_i^{(\mathrm{c})mm}(\mathbf{u}^{(\mathrm{c})},\mathbf{p}^{(\mathrm{c})})+r_i^{(\mathrm{p})ss}(\mathbf{u}^{(\mathrm{p})},\mathbf{p}^{(\mathrm{p})})]/(1+h_{ii}^{(\mathrm{c})mm}+h_{ii}^{(\mathrm{p})ss}). \tag{21}$$

From the computed sum and difference, the displacement components at the master and slave nodes can be obtained. Furthermore, the nodal tractions on the hole and pin surfaces are simply set to be zero in the separation mode by the traction-free condition.

4. Numerical results

In this section, we apply the previous iterative MLBEM to examine the problem of composite laminates with an elastically pinned circular hole. The effects of friction, bearing and bypass loading on the stress redistribution are studied in detail, based on the infinite plate configuration as shown in Fig. 1b. The issues of practical interest, such as the loading-history and cycling dependencies of stress state due to the presence of friction, are addressed. The material properties and the numerical meshes used in the simulation are described below.

The laminate plate contains seven plies of identical orthotropic material with the stacking sequence $(0/\mp 45/\overline{90})_{\mathrm{s}}$. The orthotropic material represents a unidirectional fiber-reinforced composite plate, with

the fibers lying in the horizontal plane (Lubin, 1982). The number in the stacking sequence indicates the in-plane rotation angle of each ply relative to the reference 0°-ply where the fibers lie in the 0° direction. The elastic constants are given by $E_1 = 138$ GPa, $E_2 = E_3 = 14.5$ GPa, $\mu_{23} = \mu_{13} = \mu_{12} = 5.86$ GPa, and $v_{23} = v_{13} = v_{12} = 0.21$. Meanwhile, the isotropic pin is made of Ti–6Al–4V, and the elastic constants are given by $E_f = 110$ GPa, and $v = 0.31$. The hole radius R is taken to be the normalization length scale. The plate thickness $H = 1.4R$, i.e., ply thickness $= 0.2R$. The length of the pin is $2R$.

Due to the symmetry of the configuration and materials layup relative to the horizontal middle plane, only the lower half of the plate and pin system is considered. In the resulting problem, the boundary condition at the middle plane is imposed to have zero normal displacement component and zero tangential traction components, and this condition is enforced in the fundamental solutions. Thus, the middle plane as well as the bottom surface and all interfaces of the plate are not discretized in the BE implementation; only the hole surface is discretized among the plate boundary. This results in a significant reduction of the numerical errors and size of the system of equations as compared to the FEM and the conventional BEM. Similarly, the horizontal middle plane of the pin is imposed to have zero normal displacement component and zero tangential traction components. The entire surface of the lower-half pin including the circular middle plane is discretized.

The mesh used in the simulation is described as follows. The hole surface (lower half) is discretized with 21 equal divisions in the thickness direction (i.e., six vertical divisions per ply). In the circumferential direction, 64 equal divisions are used. The elements are of the constant type, assuming uniform fields in each element and with a single node located at the center. This results in 1344 elements in total for the plate. The vertical surface of the lower-half pin is discretized with 30 equal divisions in the thickness direction and 64 equal divisions in the circumference, resulting in 1920 elements. Among these elements, those between the plate top and bottom surfaces are in one-to-one correspondence with those on the hole surface. The circular middle-plane and bottom surfaces of the pin are discretized with 177 constant elements on either one of them, as shown in Fig. 3. The total number of elements (nodes) in this coupled system is 3618. The bearing load, F, holding the pin against the hole surface, is applied to the left (opposite to the x_1-axis) uniformly on the bottom surface of the pin.

When solving this problem on a Personal Computer of 1 GHz speed, it took about 240 min to finish one run of the complete problem. However, more than one fifth of the time was spent in computing the influence coefficients. Once the influence coefficients are prepared, a series of simulations under various loading conditions but with the same geometry and materials layup, can be solved in about 20–40 min each depending on the loading conditions. Several loading cases are analyzed and discussed below.

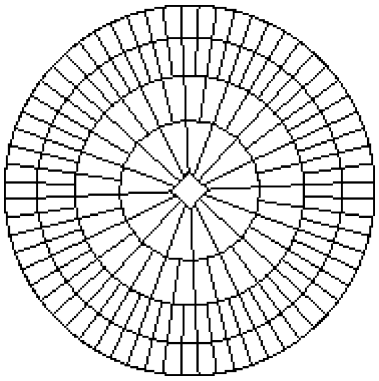

Fig. 3. Mesh on the middle plane and bottom surfaces of the pin.

4.1. Bearing load

First, a study of the case under only bearing force F, with and without friction between the plate and pin contact surfaces, is presented. In the simulation, the bearing force F was applied from zero up to $0.01\pi E_1$ in one "time" step. To check on the effects of the "time" stepping on the results, the same problem was solved in five "time" steps, finding no apparent effects. In the frictional case, the friction coefficient, f, was set to be 0.3. The contact and separation condition between the hole and pin surfaces, and variation of stress components with polar angle and with thickness along the hole edge, are plotted in Figs. 4–8.

The unfolded map of contact condition along the hole surface in the frictional case is shown in Fig. 4. The dark black color represents the stick contact mode, where the master and slave nodes stick together when moving in space and the magnitude of frictional shear traction is below the cap value of $-fp_n$ set by the friction law (Eq. (4)). The gray color represents the slip contact mode, where the master and slave nodes slide relative to each other and the magnitude of frictional shear traction reaches the cap value. Meanwhile, the white color represents the separation mode between these two surfaces. From this map, it can be seen that the hole surface and pin are in contact at polar angles from 90° to 270° and separated at the rest section. Also, the frictional contact condition in the plies exhibits a slip–stick–slip pattern, similar to but more complicated than that observed in the contact of homogeneous bodies (Hills et al., 1993). The location of the 2-D stick zone is different due to the different layered orientation in the plies and further complicated by the interaction of neighboring plies.

Fig. 5 shows the distribution of traction components versus polar angle at the middle planes of the plies at the hole edge. In the frictionless case, the contact zone is entirely in the slip contact condition, with zero tangential traction. However, in the frictional case with $f = 0.3$, the contact pressure profile is altered especially in the stick contact zone, together with the induction of non-trivial tangential traction. The induced tangential traction shows a peak of magnitude at the stick–slip boundary in the contact zone. Such variation of shear traction, coupled with the pressure, may raise the concern of developing fretting fatigue damage (Hills et al., 1993). Obviously, the contact-traction profiles in the plies are complicated, strongly dependent on the layered orientation. These complicated profiles simply suggest that neither the "cosine distribution" assumption for the pressure (Wong and Matthews, 1981; Chang, 1986) nor the 2-D plate assumption (Lin et al., 2000) would be appropriate to describe the contact behavior in the composite pinned joint. Three-dimensional stress analyses are demanded in order for an accurate assessment of strength of the composite joints.

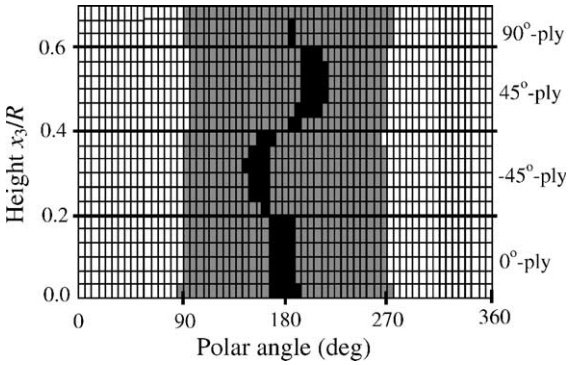

Fig. 4. Contact condition between the composite and pin under $\varepsilon_{11}^{\infty} = 0$ and $F = 0.01\pi E_1$, in the case of $f = 0.3$ (black color—stick contact zone; gray color—slip contact zone; white color—separation zone).

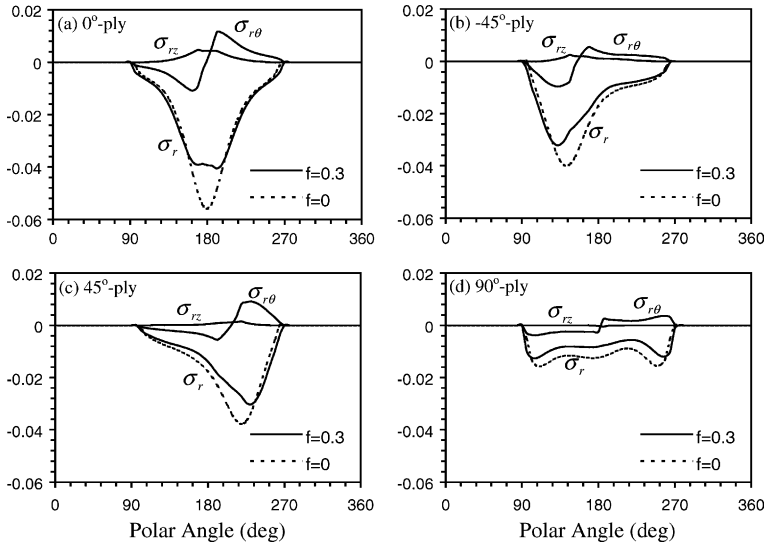

Fig. 5. Variation of the (local) contact traction components (normalized by E_1) with polar angle at the middle plane of a ply. The loads are $F = 0.01\pi E_1$ and $\varepsilon_{11}^{\infty} = 0$. The cases of $f = 0.3$ and 0 are studied for comparison. Note that in the case of $f = 0$, the tangential components $\sigma_{r\theta}$ and σ_{rz}, whose value is zero, are not shown above.

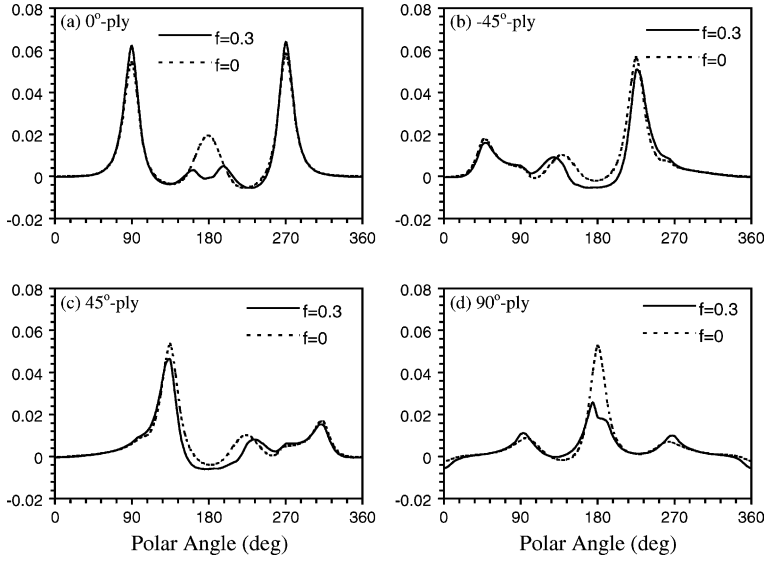

Fig. 6. Variation of the normalized hoop stress, σ_{rr}/E_1, with polar angle, at the middle plane of a ply. The loads are $F = 0.01\pi E_1$ and $\varepsilon_{11}^{\infty} = 0$. The cases of $f = 0.3$ and 0 are compared.

Fig. 6 shows the variation of hoop stress, $\sigma_{\theta\theta}$, versus polar angle at the middle plane of a ply at the hole edge. In comparison of the results with and without friction, it can be seen that the presence of friction redistributes the hoop stress in and out of the contact zone. In particular, in the 0°-ply, where the failure mode of splitting at the center of contact (i.e. at polar angle 180°) would prevail, the magnitude of the responsible hoop stress at that point is reduced significantly by the presence of the friction.

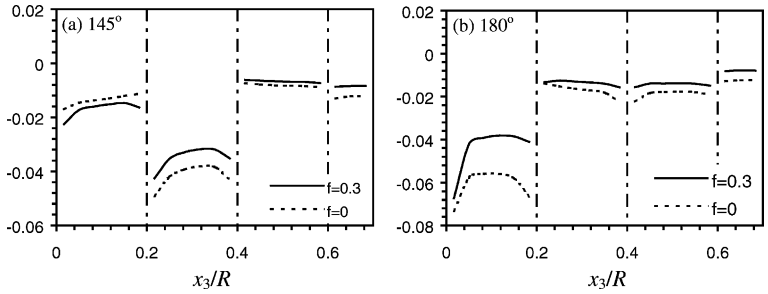

Fig. 7. Variation of the normalized normal traction component, σ_{rr}/E_1, with x_3, at two selected polar angles as indicated above. The loads are $F = 0.01\pi E_1$ and $\varepsilon_{11}^{\infty} = 0$. The cases of $f = 0.3$ and 0 are compared.

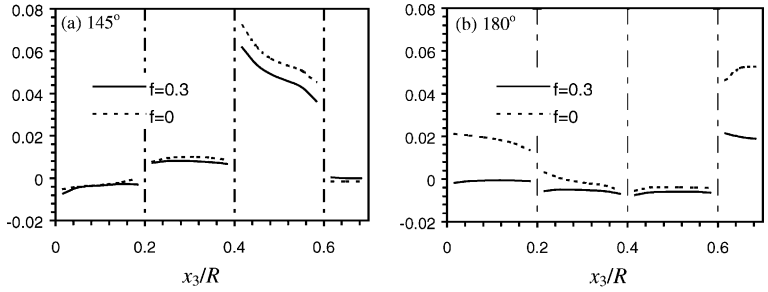

Fig. 8. Variation of the normalize hoop stress, $\sigma_{\theta\theta}/E_1$, with x_3, at selected polar angles as indicated above. The loads are $F = 0.01\pi E_1$ and $\varepsilon_{11}^{\infty} = 0$. The cases of $f = 0.3$ and 0 are compared.

The contact pressure σ_{rr} and hoop stress $\sigma_{\theta\theta}$ also are plotted versus plate thickness at polar angles 145° and 180°, as shown in Figs. 7 and 8 respectively. The both in-plane stress components vary significantly through the thickness direction, showing discontinuity across the interfaces. The contact pressure exhibits concentrations (or singularities) at the interface edges, including that at the bottom-surface edge of the 0°-ply. These variations further suggest that 3-D stress analysis is needed for the pinned joint in composite laminates.

4.2. Combined bearing and bypass loading

The configuration under both bearing force and bypass loading is more often encountered in the engineering practice of composite fastened joints than the previous situation under bearing force only. If the bypass load is comparable to the bearing force, the stress redistribution cannot be ignored, and it is critical to understand its role prior to the design of the composite joints. Below, a study of two simulations under proportional $\varepsilon_{11}^{\infty}$ and F up to 0.03 and $0.01\pi E_1$ respectively in the cases with $f = 0$ and 0.3 is presented, followed by a study of the loading-sequence and cycling effects on stress redistribution in the frictional case.

Figs. 9 and 10 show the variation of traction and hoop stress versus polar angle along the hole surface upon proportional application of $\varepsilon_{11}^{\infty}$ and F. In comparison to Figs. 5 and 6, where only the bearing force was applied, these figures show that the application of the far-field (bypass) tensile loading reduces the magnitude of contact traction in the 0°-ply but increases it in the other plies of different layered orientation.

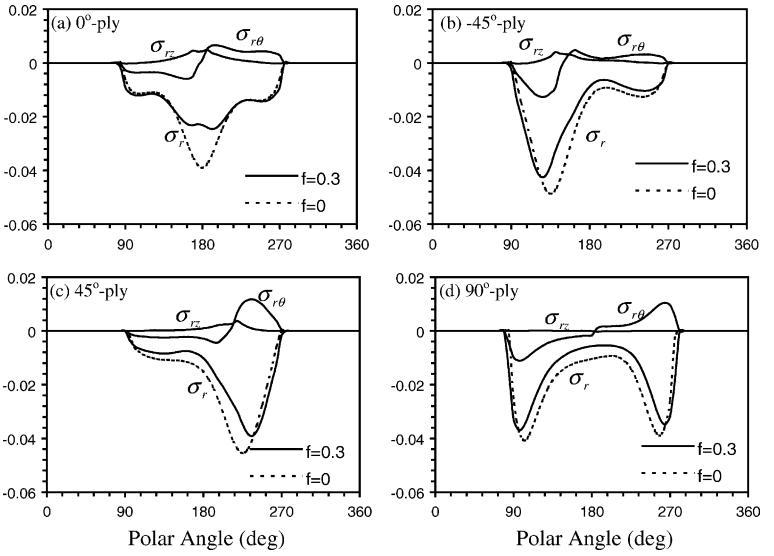

Fig. 9. Variation of the (local) traction components (normalized by E_1) with polar angle, at the middle plane of a ply. The loads are $F = 0.01\pi E_1$ and $\varepsilon_{11}^{\infty} = 0.03$. The cases of $f = 0.3$ and 0 are studied for comparison. Note that in the case of $f = 0$, the tangential components $\sigma_{r\theta}$ and σ_{rz}, whose value is zero, are not shown above.

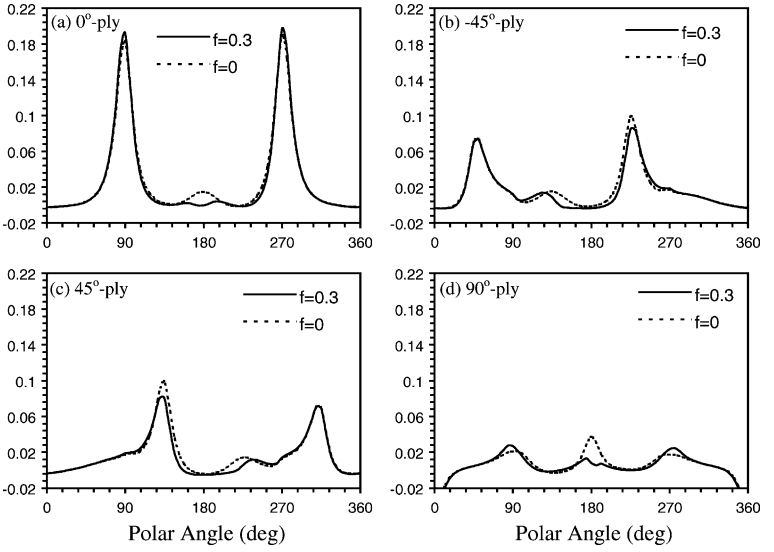

Fig. 10. Variation of the normalized hoop stress, σ_{rr}/E_1, with polar angle, at the middle plane of a ply. The loads are $F = 0.01\pi E_1$ and $\varepsilon_{11}^{\infty} = 0.03$. The cases of $f = 0.3$ and 0 are compared.

This suggests that the damage mode of bearing (Camanho and Matthews, 1997) may not always be initiated at the center of contact zone but strongly depend on the laminate layup and ratio of the bearing force to the bypass loading. In addition, the results with and without friction in comparison again show that the presence of friction suppresses the contact pressure especially in the stick contact zone while

introducing shear tractions into the system. Whether or not this is appreciable in the practice should depend on specific application cases.

As discussed before, the Coulomb-type friction model as described in Eqs. (3) and (4) is dependent on the tangent derivative of relative displacement trajectory between the contact surfaces. It may result in the dependence of final stress state on loading history. In other words, the loading sequence of applying the bearing force F and bypass loading $\varepsilon_{11}^{\infty}$ may affect the stress redistribution around the joint. In order to address this issue, two simulations were performed under the loading sequences of first applying the bearing force and then the bypass loading, and vice versa, respectively. The results are plotted in Figs. 11 and 12. Fig. 11 shows the maps of contact and separation in between the hole and pin surfaces in these two simulations together with that in the previous simulation. Fig. 12 shows the contact traction and hoop stress in the middle plane of the 0°-ply.

It can be seen that the loading sequence of applying the bearing force F and bypass loading $\varepsilon_{11}^{\infty}$ throws a significant influence on the final contact map. In the case of first applying F and then $\varepsilon_{11}^{\infty}$, the contact zone is nearly in complete slip condition. However, in the case where the loading sequence is reversed, the contact zone devotes a quite large portion to the stick contact condition. Correspondingly, the resulting traction fields yield differences especially in the tangential traction components between the two cases. The hoop stress component seems to be unaffected that much by the loading-sequence alternation.

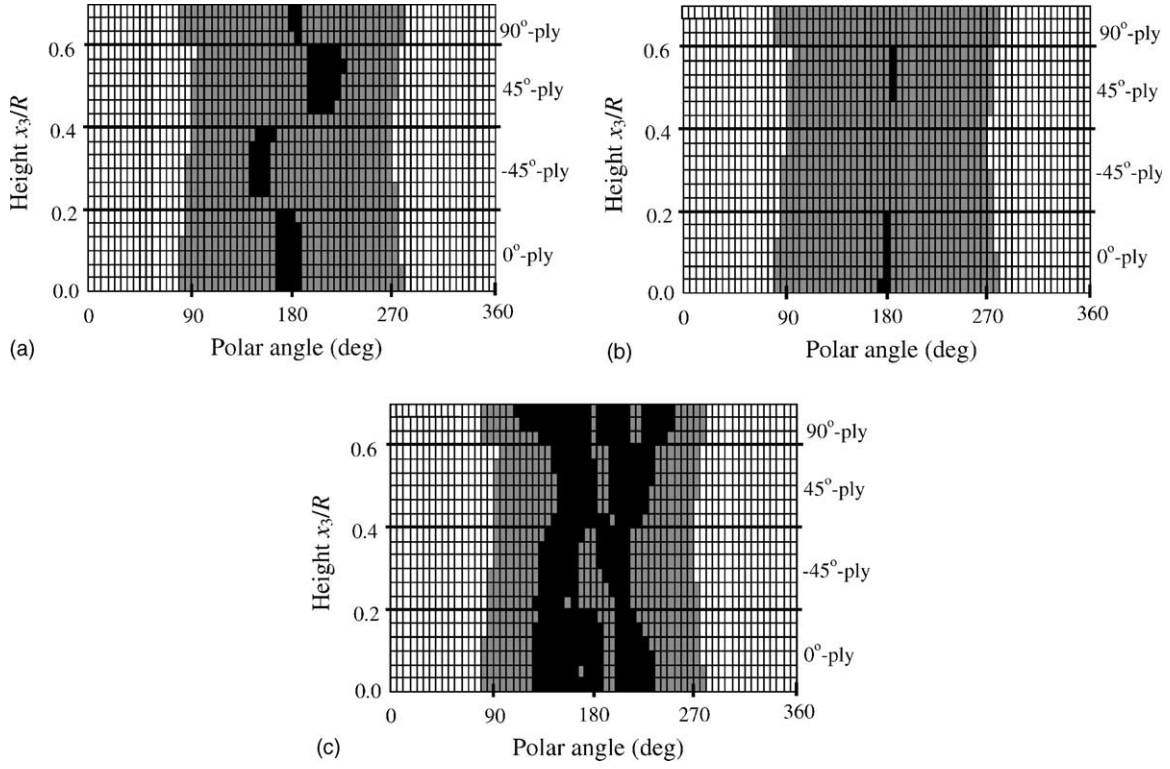

Fig. 11. Effect of loading sequence of applying the bearing force F and bypass loading $\varepsilon_{11}^{\infty}$ on contact condition between the composite and pin: (a) proportional application of F and $\varepsilon_{11}^{\infty}$; (b) application of $\varepsilon_{11}^{\infty}$ followed by F; (c) application of F followed by $\varepsilon_{11}^{\infty}$. The final $\varepsilon_{11}^{\infty} = 0.03$ and $F = 0.01\pi E_1$, with $f = 0.3$. The black color represents stick contact zone, gray color represents slip contact zone, and white color represents separation zone.

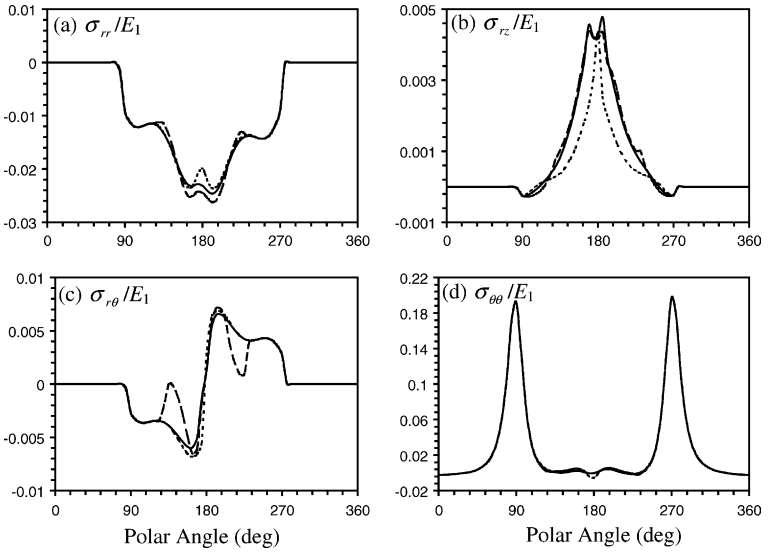

Fig. 12. Effects of loading sequence of applying the bearing force F and bypass loading $\varepsilon_{11}^{\infty}$ on contact traction (a–c) and hoop stress (d) at the middle plane of the 0°-ply. The frictional coefficient $f = 0.3$. (solid line—proportional application of F and $\varepsilon_{11}^{\infty}$; dotted line—application of $\varepsilon_{11}^{\infty}$ followed by F; dashed line—application of F followed by $\varepsilon_{11}^{\infty}$).

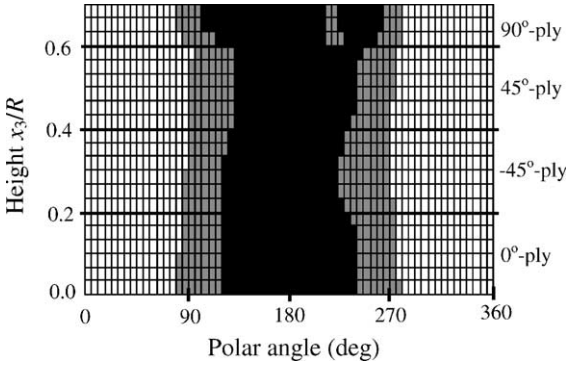

Fig. 13. Map of contact condition after five cycles of unloading and reloading in terms of $\varepsilon_{11}^{\infty}$ upon the first application of bearing force F followed by bypass straining $\varepsilon_{11}^{\infty}$. The map right before the cycling process is shown in Fig. 11c.

Finally, the cycling effect on stress redistribution in the composite joint due to the presence of friction is studied. To demonstrate this, a simulation was performed with first application of bearing force F up to $0.01\pi E_1$, followed by bypass straining $\varepsilon_{11}^{\infty}$ up to 0.03. Then, holding F at $0.01\pi E_1$, $\varepsilon_{11}^{\infty}$ was cycled between 0 and 0.03 for five cycles. The resulting map of contact condition and stress redistribution are plotted in Figs. 13 and 14. It can be seen that the load cycling changes the contact condition by expanding the contact stick zone. It also influences the stress field but in a small magnitude in the present case of perfect fitting between the hole and pin. It is expected that the cycling of load may play a significant role in stress redistribution around the composite joint if the pin shows clearance from the hole.

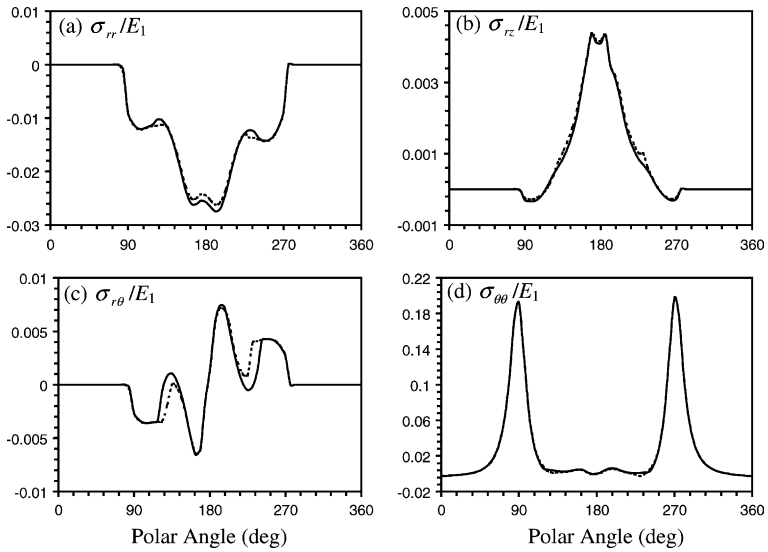

Fig. 14. Effects of load cycling on stress redistribution at the middle plane of the 0°-ply. The dotted curves represent the state at first application of $F = 0.01\pi E_1$, followed by $\varepsilon_{11}^{\infty} = 0.03$. The solid curves represent the state after five cycles of $\varepsilon_{11}^{\infty}$ between 0 and 0.03.

5. Conclusions

In this paper, we have proposed an efficient and accurate numerical method for analyzing the mechanical behavior of a composite laminate plate with an elastically pinned circular hole under a bearing force on the pin and/or bypass loading in the composite. The composite laminates are considered to be generally anisotropic and the pin to be isotropic. The plies are assumed to be perfectly bonded. The contact interaction between the composite and pin is followed by a Coulomb-type friction law. The problem is solved by using a novel 3-D boundary element formulation where the fundamental solution employs the Green's function for anisotropic multilayers that satisfies the continuity conditions of displacement and traction across the interfaces and the traction-free and symmetry conditions on the top and bottom surfaces. To simulate the non-linear frictional interaction between the composite and pin, an efficient iterative procedure with successive over-relaxation is proposed. Numerical examples are carried out for a laminate plate with the stacking sequence $(0/\mp 45/\overline{90})_s$.

It has been shown that the contact condition and stress state are complex and very different in different plies. The presence of friction in the joint reduces the magnitude of contact pressure but induces non-trivial shear traction. The distribution of other stress components is also altered. It also leads to the complicated loading-history dependence of stress state, such as dependence on loading sequence of applying the bearing force and bypass loading, and on load cycling. However, the effect of load cycling on stress redistribution is not significant in the present case of perfect fitting between the composite and pin. The traction distribution in the frictional contact zone raises the susceptibility of the pinned joint to fretting fatigue, just as in homo- geneous materials. Finally, it is remarked, based on these numerical results, that a 3-D approach to the pinned composite joints and other similar and more complicated joint geometries should be used for an accurate assessment of the strength in general.

Appendix A. Three-dimensional Green's function for anisotropic multilayers

In this section, the 3-D Green's function for anisotropic multilayers is summarized, which is derived within the framework of extended Stroh formalism and Fourier transforms. For details of the theory and computational aspects, one may refer to Ting (1996), Pan and Yuan (2000), Yuan et al. (in press), and Yang and Pan (2002), and articles cited therein.

In the formalism, the point-force Green's functions of displacement and stress first are derived in the Fourier transform domain (y_1, y_2). For a (unit) point force applied in the ith direction at $\mathbf{X}$, the solutions are given by

$$\widetilde{\mathbf{u}}^*(y_1,y_2,x_3;\mathbf{X}) = \mathrm{e}^{\mathrm{i}y_\alpha X_\alpha}\lfloor \widetilde{\mathbf{u}}^{*(\mathrm{s})}(y_1,y_2,x_3;X_3) + \mathrm{i}\eta^{-1}(\overline{\mathbf{A}}\langle \mathrm{e}^{-\mathrm{i}\bar{\mathbf{p}}\eta x_3}\rangle \mathbf{V} + \mathbf{A}\langle \mathrm{e}^{-\mathrm{i}\mathbf{p}\eta x_3}\rangle \mathbf{W})\rfloor, \tag{A.1}$$

$$\widetilde{\mathbf{t}}^*(y_1,y_2,x_3;\mathbf{X}) = \mathrm{e}^{\mathrm{i}y_\alpha X_\alpha}\lfloor \widetilde{\mathbf{t}}^{*(\mathrm{s})}(y_1,y_2,x_3;X_3) + (\overline{\mathbf{B}}\langle \mathrm{e}^{-\mathrm{i}\bar{\mathbf{p}}\eta x_3}\rangle \mathbf{V} + \mathbf{B}\langle \mathrm{e}^{-\mathrm{i}\mathbf{p}\eta x_3}\rangle \mathbf{W})\rfloor, \tag{A.2}$$

$$\widetilde{\mathbf{s}}^*(y_1,y_2,x_3;\mathbf{X}) = \mathrm{e}^{\mathrm{i}y_\alpha X_\alpha}\lfloor \widetilde{\mathbf{s}}^{*(\mathrm{s})}(y_1,y_2,x_3;X_3) + (\overline{\mathbf{C}}\langle \mathrm{e}^{-\mathrm{i}\bar{\mathbf{p}}\eta x_3}\rangle \mathbf{V} + \mathbf{C}\langle \mathrm{e}^{-\mathrm{i}\mathbf{p}\eta x_3}\rangle \mathbf{W})\rfloor, \tag{A.3}$$

where $\mathbf{u}^* \equiv u^*_{ji}$, $\mathbf{t}^* \equiv (\sigma^*_{13i}, \sigma^*_{23i}, \sigma^*_{33i})$, $\mathbf{s}^* \equiv (\sigma^*_{11i}, \sigma^*_{12i}, \sigma^*_{22i})$, η together with θ are the polar coordinates of (y_1, y_2), the superscript (s) indicates a given special solution, and tensors $\mathbf{V}$ and $\mathbf{W}$ are unknowns to be determined by boundary conditions. The special solutions may be given to be the infinite-space Green's function (Tonon et al., 2001) or the bimaterial Green's function (Pan and Yuan, 2000). The eigenvalues p_i and eigenmatrix $\mathbf{A} = (\mathbf{a_1}, \mathbf{a_2}, \mathbf{a_3})$ are related by the following Stroh eigenrelation in an oblique plane spanned by $(n_1 = \cos\theta, n_2 = \sin\theta, 0)^{\mathrm{T}}$ and $(0,0,1)^{\mathrm{T}}$, as

$$[\mathbf{Q} + p_i(\mathbf{R} + \mathbf{R}^{\mathrm{T}}) + p_i^2\mathbf{T}]\mathbf{a}_i = 0, \tag{A.4}$$

with

$$Q_{ik} = C_{i\alpha k\beta}n_\alpha n_\beta, \quad R_{ik} = C_{i\alpha k3}n_\alpha, \quad \text{and} \quad T_{ik} = C_{i3k3}. \tag{A.5}$$

The matrix $\mathbf{B}$ and $\mathbf{C}$ are related to $\mathbf{A}$ and the elastic constants (Ting, 1996).

The above expressions of displacement and stress are valid for a homogeneous domain. In the multilayer system of different homogeneous layers, the unknown tensors $\mathbf{V}$ and $\mathbf{W}$ for every layer can be derived by assigning Eqs. (A.1) and (A.2) to different layers and enforcing the interfacial continuity conditions of displacement and traction and top- and bottom-surface boundary conditions. In our case of composite laminates of symmetry relative to the horizontal middle plane, the interfacial and boundary conditions are given by

$$\mathbf{t} = 0, \quad \text{at } x_3 = h_0, \tag{A.6}$$

$$\mathbf{u}_m = \mathbf{u}_{m+1} \quad \text{and} \quad \mathbf{t}_m = \mathbf{t}_{m+1}, \quad \text{at } x_3 = h_m, \quad \text{for } m = 1,\ldots,M-1, \tag{A.7}$$

$$t_1 = t_2 = u_3 = 0, \quad \text{at } x_3 = h_M, \tag{A.8}$$

where m indicates the attachment to the mth layer, M is the number of layers, and h_m is the vertical level of the interfaces including the top and bottom surfaces. Substituting the expressions of displacement and stress in the transform-domain version of the above equations, one obtains

$$\widetilde{\mathbf{t}}_1^{*(\mathrm{s})}(h_0) + (\overline{\mathbf{B}}_1\mathbf{V}_1 + \mathbf{B}_1\langle \mathrm{e}^{-\mathrm{i}\mathbf{p}_1\eta(h_0-h_1)}\rangle \mathbf{W}_1) = 0, \tag{A.9}$$

$$\begin{aligned}&\widetilde{\mathbf{u}}_m^{*(\mathrm{s})}(h_m) + \mathrm{i}\eta^{-1}(\overline{\mathbf{A}}_m\langle \mathrm{e}^{-\mathrm{i}\bar{\mathbf{p}}_m\eta(h_m-h_{m-1})}\rangle \mathbf{V}_m + \mathbf{A}_m\mathbf{W}_m)\\ &\quad = \widetilde{\mathbf{u}}_{m+1}^{*(\mathrm{s})}(h_m) + \mathrm{i}\eta^{-1}(\overline{\mathbf{A}}_{m+1}\mathbf{V}_{m+1} + \mathbf{A}_{m+1}\langle \mathrm{e}^{-\mathrm{i}\mathbf{p}_{m+1}\eta(h_m-h_{m+1})}\rangle \mathbf{W}_{m+1}), \quad \text{for } m = 1,\ldots,M-1,\end{aligned} \tag{A.10}$$

$$\widetilde{\mathbf{t}}_m^{*(s)}(h_m) + (\overline{\mathbf{B}}_m \langle e^{-i\bar{p}_m \eta (h_m - h_{m-1})} \rangle \mathbf{V}_m + \mathbf{B}_m \mathbf{W}_m) = \widetilde{\mathbf{t}}_{m+1}^{*(s)}(h_m) + (\overline{\mathbf{B}}_{m+1} \mathbf{V}_{m+1} + \mathbf{B}_{m+1} \langle e^{-i\bar{p}_{m+1} \eta (h_m - h_{m+1})} \rangle \mathbf{W}_{m+1}),$$
$$\text{for } m = 1, \ldots, M-1, \tag{A.11}$$

$$\widetilde{\mathbf{g}}_M^{*(s)}(h_M) + (\overline{\mathbf{G}}_M \langle e^{-i\bar{p}_M \eta (h_M - h_{M-1})} \rangle \mathbf{V}_M + \mathbf{G}_M \mathbf{W}_M) = 0. \tag{A.12}$$

In Eq. (A.12), $\widetilde{\mathbf{g}}^*$ and $\mathbf{G}$ are defined by

$$\widetilde{\mathbf{g}}^* \equiv \begin{pmatrix} t_{11}^* & t_{12}^* & t_{13}^* \\ t_{21}^* & t_{22}^* & t_{23}^* \\ u_{31}^* & u_{32}^* & u_{33}^* \end{pmatrix} \quad \text{and} \quad \mathbf{G} \equiv \begin{pmatrix} B_{11} & B_{12} & B_{13} \\ B_{21} & B_{22} & B_{23} \\ i\eta^{-1} A_{31} & i\eta^{-1} A_{32} & i\eta^{-1} A_{33} \end{pmatrix}. \tag{A.13}$$

Eqs. (A.9)–(A.12) form a linear system of $2M$ algebraic equations with $2M$ unknowns of $\mathbf{V}_m$ and $\mathbf{W}_m$. Therefore, $\mathbf{V}_m$ and $\mathbf{W}_m$ $(m = 1, \ldots, M)$ can be determined for each given set of y_1, y_2 and X_3 by solving this system of equations. Subsequently, the Green's displacement and stress are obtained in the transform domain.

Upon the derivation of the Green's functions in the transform domain, the physical Green's functions are evaluated by the Fourier inverse transform over the infinite plane (y_1, y_2). This has been implemented using an adaptive quadrature procedure. The efficiency of the evaluation may be dependent on the choice of the special solutions. These numerical issues are not discussed in the present paper; one may refer to the articles mentioned earlier.

References

Brebbia, C.A., Telles, J.C.F., Wrobel, L.C., 1984. Boundary Element Techniques: Theory and Applications in Engineering. Springer-Verlag.

Camanho, P.P., Matthews, F.L., 1997. Stress analysis and strength prediction of mechanically fastened joints in FRP: a review. Composites Part A. 28A, 529–547.

Chang, F.K., 1986. The effect of pin load distribution on the strength of pin loaded holes in laminated composites. Journal of Composite Materials 20, 401–408.

Chen, W.H., Lee, S.S., Yeh, J.T., 1995. Three-dimensional contact stress analysis of a composite laminate with bolted joint. Composite Structures 30, 287–297.

Daniel, I.M., Rowlands, R.E., Whiteside, J.B., 1974. Effects of material and stacking sequence on behavior of composite plates with holes. Experimental Mechanics 14, 1–9.

Dano, M.L., Gendron, G., Picard, A., 2000. Stress and failure analysis of mechanically fastened joints in composite laminates. Composite Structures 50, 287–296.

Hills, D.A., Nowell, D., Sackfield, A., 1993. Mechanics of Elastic Contacts. Butterworth-Heinemann Ltd., Oxford, UK.

Iarve, E.V., 1996. Spline variational three-dimensional stress analysis of laminated composite plates with open holes. International Journal of Solids and Structures 33, 2095–2118.

Iarve, E.V., 1997. Three-dimensional stress analysis in laminated composites with pins based on the B-spline approximation. Composites Part A 28, 559–571.

Ireman, T., 1998. Three-dimensional stress analysis of bolted single-lap composite joints. Composite Structures 43, 195–216.

Ireman, T., Ranvik, T., Eriksson, I., 2000. On damage development in mechanically fastened composite laminates. Composite Structures 49, 151–171.

Lie, S.T., Yu, G., Zhao, Z., 2000. Analysis of mechanically fastened composite joints by boundary element methods. Composites Part B 31, 693–705.

Lin, C.C., Lin, C.H., Wang, J.T.S., 2000. On some aspects of pin-loaded laminates. International Journal of Solids and Structures 37, 599–625.

Love, A.E.H., 1944. A Treatise on the Mathematical Theory of Elasticity. Dover, New York.

Lubin, G., 1982. Handbook of Composites. Van Nostrand Reinhold Company, New York.

Marshall, I.H., Arnold, W.S., Wood, J., Mousley, R.F., 1989. Observations on bolted connections in composite structures. Composite Structures 13, 133–151.

Merkel, M., Bulgakov, V., Bialecki, R., Kuhn, G., 1998. Iterative solution of large-scale 3D-BEM industrial problems. Engineering Analysis with Boundary Elements 22, 183–197.

Nishioka, T., Atluri, S.N., 1982. Stress analysis of holes in angle-ply laminates: An efficient assumed stress special-hole-element approach and a simple estimation method. Computers and Structures 15, 135–147.

Pan, E., Yuan, F.G., 2000. Three-dimensional Green's functions in anisotropic bimaterials. International Journal of Solids and Structures 37, 5329–5351.

Pan, E., Yang, B., Cai, G., Yuan, F.G., 2001. Stress analyses around holes in composite laminates using boundary element method. Engineering Analysis with Boundary Elements 25, 31–40.

Persson, E., Madenci, E., Eriksson, I., 1998. Delamination initiation of laminates with pin-loaded holes. Theoretical and Applied Fracture Mechanics 30, 87–101.

Raju, I.S., Crews Jr., J.H., 1982. Three-dimensional analysis of $[0/90]_s$ and $[90/0]_s$ laminates with a central circular hole. Composites Technology Review 4, 116–124.

Rybicki, E.F., Hopper, A.T., 1973. Analytical investigation of stress concentration due to holes in fiber reinforced plastic laminated plates: three-dimensional models. AFML-TR-73-100, Battelle Columbus labs.

Rybicki, E.F., Schmuesser, D.W., 1976. Three-dimensional finite element stress analysis of laminated plates containing a circular hole. AFML-TR-76-92, Battelle Columbus Labs.

Schwartz, M.M., 1984. Composite Materials Handbook. McGraw-Hill Book Company, New York.

Soni, S.R., 1981. Stress and strength analysis of bolted joints in composite laminates. In: Marshall, I.H. (Ed.), Composite Structures. Applied Science Publishers, New York, pp. 50–62.

Tang, S., 1977. Interlaminar stresses around circular cutouts in composites plates under tension. AIAA Journal 15, 1631–1637.

Tang, S., 1979. A variational approach to edge stresses of circular cutouts in composites. In: AIAA Paper 79-0802, 20th AIAA/ASME/ASCE/AHS, SDM Conference, St. Louis, MO. pp. 326–332.

Ting, T.C.T., 1996. Anisotropic Elasticity. Oxford University, Oxford.

Tonon, F., Pan, E., Amadei, B., 2001. Green's functions and boundary element formulation for 3D anisotropic media. Computers and Structures 79, 469–482.

Waszczak, J.P., Cruse, T.A., 1971. Failure mode and strength predictions of anisotropic bolt bearing specimens. Journal of Composite Materials 5, 421–425.

Wong, S., Matthews, F.L., 1981. A finite element analysis of single and two-hole bolted joints in fibre reinforced elastic. Journal of Composite Materials 15, 481–491.

Yang, B., Mall, S., Ravi-Chandar, K., 2001. A cohesive zone model of fatigue crack growth in quasibrittle materials. International Journal of Solids and Structures 38, 3927–3944.

Yang, B., Pan, E., 2002. Efficient evaluation of three-dimensional Green's functions in anisotropic elastostatic multilayered composites. Engineering Analysis with Boundary Elements 26, 355–366.

Yang, B., Ravi-Chandar, K., 1998. A single-domain dual-boundary-element formulation incorporating a cohesive zone model for elastostatic cracks. International Journal of Fracture 93, 115–144.

Yuan, F.G., Yang, S., Yang B. Three-dimensional Green's functions for composite laminates. International Journal of Solids and Structures, in press.